Journal of Advanced Biomedical Sciences

https://jabs.fums.ac.ir/
Online ISSN: 2783-1523

Journal of Advanced Biomedical Sciences

Fasa University of Medical Sciences

Downloaded from jabs.fums.ac.ir at 7:25 +0330 on Sunday November 29th 2026

In Silico Evaluation of the Conformational Selectivity of Curcumin and Rosmarinic Acid Derivatives for Tense and Relaxed States of Sickle Cell Hemoglobin

Roohallah Yousefi[1], Seyed Hossein Khaleghinejad[2], Dariush Gholami[2], Sadegh Hasannia[1]

1. Department of Biochemistry, Faculty of Biology, Tarbiat Modares University of Tehran, Tehran, Iran
2. Department of Bioinformatics and Applied Biotechnology, Faculty of Biotechnology, Amol University of Special Modern Technologies, Amol, Iran

Article Info

Article Type:
Original Article

Article history:
Received
15 Jul 2026
Received in revised form
24 Aug 2026
Accepted
01 Sep 2026
Published online
10 Sep 2026

Publisher
Fasa University of Medical Sciences

Abstract

Background & Objective: Sickle cell disease (SCD) arises from the polymerization of hemoglobin S (HbS) under low-oxygen conditions, leading to vaso-occlusion and organ damage. This study evaluated the binding and interaction profiles of curcumin and rosmarinic acid in comparison with voxelotor across different HbS conformations.

Materials & Methods: Molecular docking was performed using Molegro Virtual Docker (MVD) with the MolDock Scoring algorithm. Two HbS models were used: the relaxed state (PDB ID: 5E83) and the tense state (PDB ID: 2HBS). The docking protocol was validated by redocking the co-crystallized ligand, with an RMSD threshold of < 3.8 Å. Binding affinities were compared between the R2 and T states to assess conformational selectivity.

Results: Analysis of ligand-binding profiles in the R2 (−149.57) and T (−118.84) conformations of HbS revealed marked differences. Rosmarinic acid and curcumin preferentially bound to the R2 state, as indicated by their more favorable binding scores, greater hydrogen-bonding interactions, and interaction energies. Voxelotor also exhibited a more favorable score in R2 than in T (−122.39 vs. −109.27). Although the T state exhibited stronger individual interactions, the overall interaction profiles were less extensive. In contrast, the R2 state provided a more favorable binding environment for multiple ligands. The findings are consistent with the Monod-Wyman-Changeux allosteric model and suggest that the R2 state provides a more favorable physicochemical environment for ligand accommodation. The transition from T to R2 involves a redistribution of energetic hotspots, with the principal interactions for rosmarinic acid shifting from Arg141 and Thr137 toward Lys99 and His103. These findings highlight the importance of steric complementarity and van der Waals forces, in addition to hydrogen bonding, in effective allosteric stabilization.

Conclusion: This study suggests that the R2 conformation of HbS provides a more favorable binding environment for the investigated natural polyphenols and synthetic ligands. These results provide a computational basis for designing novel antisickling agents that selectively stabilize the relaxed state to mitigate SCD pathology.

Keywords: Sickle Cell Disease, Hemoglobin S, Molecular Docking, Protein Conformation, Curcumin

Cite this article: Yousefi R, Khaleghinejad S.H, Gholami D, Hasannia S. *In Silico* Evaluation of the Conformational Selectivity of Curcumin and Rosmarinic Acid Derivatives for Tense and Relaxed States of Sickle Cell Hemoglobin. J Adv Biomed Sci. 2026; 16(4): 325-347.
DOI: 10.18502/jabs.v16i4.22275

Corresponding Author: Seyed Hossein Khaleghinejad, Department of Bioinformatics and Applied Biotechnology, Faculty of Biotechnology, Amol University of Special Modern Technologies, Amol, Iran.
Email: hosseinkhaleghi403@ausmt.ac.irc

Introduction

Sickle cell disease (SCD) is a severe genetic blood disorder caused by the polymerization of mutated hemoglobin S (HbS) under deoxygenated conditions (1). This pathological polymerization causes red blood cells to assume

[DOI: 10.18502/jabs.v16i4.22275]
Downloaded from jabs.fums.ac.ir at 7:25 +0330 on Sunday November 29th 2026

a rigid, sickle-shaped morphology, resulting in vaso-occlusion, chronic pain, and progressive organ damage (1). To address this condition, modern drug discovery frequently relies on structure-based computational methods to identify molecules capable of modulating specific protein conformations (2). Molecular docking serves as an essential preliminary step in this process by predicting the optimal binding configurations and affinities of small-molecule ligands within target protein-binding sites (3, 4). Among potential structural targets, stabilization of the oxygenated, relaxed (R2) state of HbS over the deoxygenated, tense (T) state represents a key therapeutic strategy for preventing HbS polymerization. Despite its importance, molecular docking remains challenging when binding poses must be predicted across highly dynamic protein conformations (4). Conventional and deep-learning-based approaches often face challenges associated with extensive conformational search spaces and substantial computational requirements for accurately sampling ligand-binding poses (2, 5).

Aromatic aldehydes have been shown to enhance the oxygen-carrying capacity of hemoglobin. Studies have demonstrated that certain vanillin derivatives, including 5HMF and INN-312, possess potent antisickling properties. INN-312 interacts with the alpha chain of hemoglobin, reducing sickling by inhibiting HbS polymerization (6, 7). By stabilizing HbS in the R state, aromatic aldehydes increase oxygen affinity and may prevent HbS polymerization under hypoxic conditions (8, 9). Voxelotor (GBT-440) inhibits HbS polymerization and red blood cell (RBC) sickling, potentially benefiting patients with SCD by reducing blood viscosity. Both vanillin and GBT-440 form Schiff-base linkages with the alpha chain of HbS, and their distinct binding patterns have been elucidated through X-ray analysis (10-15).

Therefore, evaluating natural compounds with favorable stereochemical compatibility across different allosteric states is warranted (2-5). In this study, we examined the binding affinities and interaction patterns of curcumin and rosmarinic acid with a sickle hemoglobin (HbS) model and compared their binding profiles with that of voxelotor (GBT-440), with particular emphasis on key amino acid residues. We also investigated the effects of HbS conformation by comparing the R2 and T states. These findings may help elucidate how conformational changes in the HbS model influence the binding affinities of the investigated ligands.

Materials and Methods

Literature Review

A literature review was conducted to evaluate the use of natural compounds that interact with sickle cell hemoglobin (HbS) and to compare their binding affinities in the R2 state with those in the T state. The review involved searching several databases, including PubMed, ScienceDirect, and Scopus, using relevant keywords such as hemoglobin, hemoglobinopathy, sickle cell disease, aromatic aldehydes, and antisickling agents.

Model Preparation

The crystal structure of carbonmonoxy hemoglobin S complexed with GBT-440 (PDB ID: 5E83) was determined by X-ray diffraction at a resolution of 1.8 Å. Crystallization was performed by vapor diffusion using a solution containing 0.1 M HEPES (pH 7.4), 25% PEG 4000, and 40 mM NaCl at 294 K. The orthorhombic crystal system had a space group of P 21 21 21 and unit-cell dimensions of a = 58.777 Å, b = 59.104 Å, and c = 170.26 Å. The diffraction data collected at NSLS beamline X29A were 99.1% complete. The structure was determined by molecular replacement using PDB entry 1NEJ, with 53,969 reflections yielding R-work and R-free values of 0.1773 and 0.2075, respectively. Binding of GBT-440 stabilizes the CO-bound hemoglobin S fiber tetramer, a feature relevant to the development of therapies for SCD.

[DOI: 10.18502/jabs.v16i4.22275]
Downloaded from jabs.fums.ac.ir at 7:25 +0330 on Sunday November 29th 2026

The structure with PDB ID 5E83 was retrieved from https://www.rcsb.org/structure/5E83 (16).

The structure with PDB ID 2HBS was determined using X-ray diffraction at a resolution of 2.05 Å. Deoxyhemoglobin S is a hemoglobin variant characterized by the βGlu6Val mutation. The crystal structure was refined to an R-factor of 16.5% and a free R-value of 21.5%. A key finding was the identification of a double-stranded arrangement of hemoglobin tetramers, which serves as the fundamental building block of sickle cell fibers. This double-stranded configuration is stabilized by interactions between the mutant valine residues and adjacent hemoglobin tetramers. Specifically, the βGlu6→Val mutation introduces a hydrophobic valine residue that promotes the pathological polymerization of hemoglobin S through lateral contacts between tetramers, resulting in the formation of double-stranded fibers characteristic of SCD. The refined structure revealed conformational shifts of approximately 3.5 Å in lateral-contact residues compared with earlier, lower-resolution models, underscoring the dynamic nature of these interactions. The structure was deposited by Harrington, Adachi, and Royer Jr. on May 6, 1997, and released on July 23, 1997. For the docking studies, the deoxygenated hemoglobin tetramer was extracted from PDB ID 2HBS to represent the T conformation of HbS (9).

The structures of vanillin, INN-312, and GBT-440 were obtained from the PubChem database. Molegro Virtual Docker was used to prepare the selected molecules. The hemoglobin model comprised an alpha-beta globin tetramer. Ions and water molecules were removed from the hemoglobin structure, and residue deprotonation was performed automatically using the software (16).

Molecular Docking

Molecular docking was performed using Molegro Virtual Docker (MVD) to predict the binding modes and interaction profiles of the selected ligands with the target proteins. The software provides flexible docking capabilities, allowing different ligand and receptor conformations to be considered during the docking process (17-19). MVD features grid-based scoring functions, multiple docking engines, and comprehensive output-analysis tools. In the Docking Wizard, we selected the MolDock Scoring Grid algorithm with a grid resolution of 0.3 Å. To optimize ligand energies, we used the MolDock SE algorithm with 1,500 iterations per run and 10 runs for each ligand-receptor docking simulation.

For blind docking, the search space for the prepared target structure (PDB ID: 5E83) was centered at X = 15.68, Y = 0.25, and Z = −21.31, with a radius of 21 Å. The binding-site grid for the prepared target structure (PDB ID: 2HBS) was also configured, with the search space centered at X = 5.75, Y = 25.42, and Z = 32.05 and a radius of 21 Å. This configuration covered the entire protein molecule, allowing the identification of potential binding sites across the hemoglobin structure. Hydrophobic compounds interact with the hydrophobic cavity and the interchain and intrachain clefts of hemoglobin tetramers, thereby contributing to favorable binding energies. The graphical user interface (GUI) of Molegro Virtual Docker (v5.0) allows visualization of ligand-receptor interactions and the energy contributions associated with different atom pairs. Users can switch between tabular and three-dimensional views to gain a better understanding of complex interactions. Energy types include EPair (interactions between ligand and receptor atoms), EIntra (internal ligand energy), and EElec (electrostatic interactions). The software distinguishes between short-range and long-range interactions, which are important for evaluating the stability of ligand-receptor complexes.

Prior to docking, all crystallographic water molecules and ions were removed, and the protein structures were prepared according to the recommended protocol. This preparation included assigning protonation states, adding

[DOI: 10.18502/jabs.v16i4.22275]
Downloaded from jabs.fums.ac.ir at 7:25 +0330 on Sunday November 29th 2026

hydrogen atoms, and automatically removing nonpolar hydrogen atoms to ensure the consistency of the docking simulations. All ligands were docked under identical conditions, including the same number of iterations and software parameters (18, 20-22).

Docking Validation and Binding Affinity Accuracy with MolDock Scoring

To validate the docking protocol, the co-crystallized ligand was removed from the HbS-R2 structure (PDB ID: 5E83) and subsequently redocked using Molegro Virtual Docker (MVD). The redocked pose was compared with the original crystallographic pose by calculating the root mean square deviation (RMSD). An RMSD value of < 3.0 Å was considered indicative of successful reproduction of the experimental binding mode and was used to validate the docking protocol (Supplementary Appendices 1 and 2).

Cross-docking was also performed by docking a ligand extracted from a co-crystal structure into a different conformation of the same protein rather than into its native holo structure. For this purpose, we used the sickle hemoglobin model in the tense (T) state. Voxelotor was extracted from PDB ID 5E83, which represents HbS in the R2 conformation, and then docked into the T state derived from the primary study model (PDB ID 2HBS). Docking simulations were conducted using the prepared models and the ligands under investigation. Finally, the binding affinities and binding sites of the ligands were compared between the two HbS conformations, namely, the relaxed (R2) and tense (T) states (9, 23-29).

Results

Comparative Analysis of Ligand Binding Profiles in R2 and T Conformations of HbS

Docking analysis revealed distinct predicted ligand-binding profiles between the relaxed (R2) and tense (T) conformations of HbS. Rosmarinic acid exhibited a more favorable predicted MolDock score in the R2 conformation (−149.57) than in the T conformation (−118.84). This difference was associated with a greater contribution from hydrogen bonding in R2 (−13.24) than in T (−9.34), together with a more favorable predicted protein-ligand interaction energy (−165.77 versus −134.13, respectively). A similar trend was observed for curcumin, which exhibited a more favorable predicted MolDock score in R2 (−149.30) than in T (−136.59), accompanied by a lower predicted internal energy in R2 (1.13) than in T (12.92).

Voxelotor and the smaller ligands exhibited distinct predicted interaction patterns across the two conformational states. Voxelotor showed a more favorable predicted MolDock score in R2 (−122.39) than in T (−109.28), accompanied by an additional predicted cofactor-interaction contribution in the R2 conformation (−0.18). In contrast, vanillin exhibited comparable predicted MolDock scores in the two states (−73.24 in R2 versus −70.62 in T), suggesting that its predicted binding profile was relatively independent of the HbS conformation.

Notably, CID 162739375 exhibited a more favorable predicted MolDock score in R2 (−135.97) than in T (−117.70). Although its predicted internal energy was higher in R2 (20.06), the ligand retained a favorable overall predicted docking score. Its relatively high heavy-atom count (22) and molecular weight (300.31 Da) may facilitate multiple contacts within the R2 binding environment, consistent with the predicted stabilization of a comparatively large molecular scaffold.

Overall, most of the investigated ligands exhibited more favorable predicted MolDock scores in the R2 conformation than in the T state, although the magnitude and energetic basis of this preference varied among compounds. CID 141386569 showed a pronounced preference for R2, with a predicted MolDock score of −124.04 compared with −95.48 in T. This preference was accompanied by greater predicted ligand efficiency in R2 (−5.39 MolDock score per heavy atom) than in T (−4.15 MolDock score per heavy atom).

Downloaded from jabs.fums.ac.ir at 7:25 +0330 on Sunday November 29th 2026 [DOI: 10.18502/jabs.v16i4.22275]

Table 1. presents the docking results for the studied compounds on different HBS conformation models, including [PDB ID: 5E83] (R2) and [PDB ID: 2HBS] (T).

Ligand-Target	Ligand CID Number	MolDock Score (MolDock Score)	Rerank Score (MolDock Score)	Inter-action (Total inter-action energy between POS and tar-get)	Cofactor (POS-Cofactor energy interac-tions.) (MolDock Score)	Protein (POS-Protein interaction) (MolDock Score)	Internal (POS interaction energy) (MolDock Score)	Tor-sions	H Bond	Heavy Atoms	MW	LE1 (MolDock Score/ Heavy Atoms)	Docking Score (MolDock Score)
Rosmarinic Acid -HBS (R2)	5315615	-149.57	-88.71	-165.77	-0.76	-165.01	16.19	7	-13.24	26	360.32	-5.753	-155.80
Rosmarinic Acid-HBS (T)	5315615	-118.84	-92.88	-134.13	-0.67	-133.46	15.29	7	-9.34	26	360.32	-4.57	-124.08
Curcumin-HBS (T)	969516	-136.59	-97.60	-149.52	0	-149.52	12.92	8	-6.88	27	370.40	-5.06	-138.94
Curcumin-HBS (R2)	969516	-149.30	-94.73	-150.43	0	-150.43	1.13	8	-5.21	27	370.40	-5.53	-140.00
Voxelotor-HBS (R2)	71602803	-122.39	-90.25	-134.79	-0.18	-134.61	12.40	6	-5.27	25	338.38	-4.90	-127.31
Voxelotor-HBS (T)	71602803	-109.28	-65.00	-123.48	0	-123.48	14.21	6	-11.32	25	338.38	-4.371	-114.75
162739375-HBS (R2)	162739375	-135.97	-98.82	-156.03	0	-156.03	20.06	6	-9.35	22	300.31	-6.18	-133.37
162739375-HBS (T)	162739375	-117.70	-94.96	-132.40	0	-132.40	14.71	6	-9.23	22	300.31	-5.35	-122.84
141386569-HBS (R2)	141386569	-124.04	-103.08	-148.45	0	-148.45	24.41	6	-8.48	23	322.35	-5.39	-123.96
141386569-HBS (T)	141386569	-95.48	-78.91	-110.00	0	-110.00	14.52	6	-8.71	23	322.35	-4.15	-98.05
24015539-HBS (T)	24015539	-104.89	-77.28	-106.47	0	-106.47	1.576	5	-13.39	20	274.27	-5.24	-112.10
24015539-HBS (R2)	24015539	-117.91	-96.71	-131.63	0	-131.63	13.71	5	-8.30	20	274.30	-5.90	-123.60
Vanillin-HBS (R2)	1183	-73.24	-58.78	-80.16	0	-80.16	6.92	2	-9.53	11	153.16	-6.66	-76.04
Vanillin-HBS (T)	1183	-70.62	-56.76	-75.16	0	-75.16	4.54	2	-8.09	11	153.16	-6.42	-76.09

Journal of Advanced Biomedical Sciences
Fasa University of Medical Sciences

[DOI: 10.18502/jabs.v16i4.22275]
Downloaded from jabs.fums.ac.ir at 7:25 +0330 on Sunday November 29th 2026

CID 24015539 also exhibited a more favorable predicted MolDock score in R2 (−117.91) than in T (−104.89), despite a less favorable predicted hydrogen-bond contribution in R2 (−8.30) than in T (−13.39). These findings suggest that factors beyond hydrogen bonding, including steric complementarity, electrostatic interactions, and other intermolecular contributions, may account for differences in predicted binding scores between the two conformational states (Table 1 and Figure 1).

Comparative Analysis of Rosmarinic Acid Interactions with Tense and R2 Conformations of HbS

Comparative analysis of rosmarinic acid binding revealed pronounced differences in hydrogen-bonding, electrostatic, residue-level, and atomic interaction patterns between the T (tense) and R2 (relaxed) conformations of HbS, indicating substantial remodeling of the binding environment during the transition from T to R2. In the T conformation, rosmarinic acid formed nine interactions, including two electrostatic contacts (IDs 0 and 1) and seven hydrogen bonds involving different donor configurations, with the ligand, the target, or either serving as the hydrogen-bond donor. Three hydrogen bonds (IDs 2, 6, and 7) exhibited the most favorable hydrogen-bond energy of −2.50 MolDock score, with highly favorable donor-hydrogen-acceptor (D-H-A) angles of 168.6°, 164.9°, and 158.1°, respectively, and bond lengths ranging from

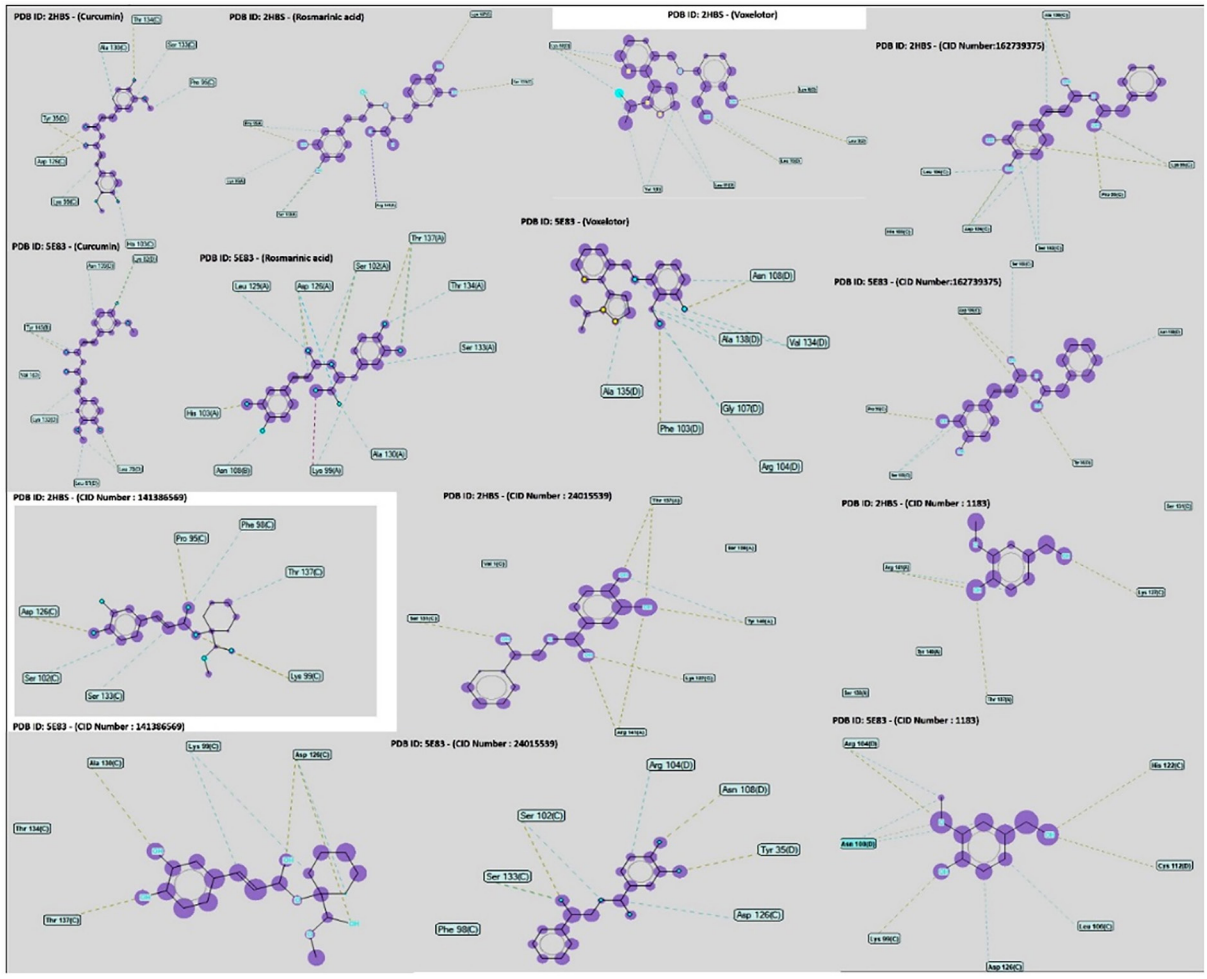


Figure 1. 2D Ligand map of studied compounds in complex by HBS hemoglobin model [PDB ID: 5E83 (R2)]; [PDB ID:2HBS (T)].

[DOI: 10.18502/jabs.v16i4.22275]
Downloaded from jabs.fums.ac.ir at 7:25 +0330 on Sunday November 29th 2026

2.85 to 3.37 Å, indicating strong directional interactions. Electrostatic contacts were comparatively weak, contributing −1.41 and −1.10 MolDock score at distances of 3.84 and 4.35 Å, respectively.

In contrast, rosmarinic acid formed a more extensive interaction network in the R2 conformation, comprising eleven interactions, including four electrostatic contacts and seven hydrogen bonds. Hydrogen bonds with IDs 4 and 5 also reached the most favorable energy value (−2.50 MolDock score), whereas those with IDs 8 (−2.21) and 1 (−1.84 MolDock score) provided additional stabilization, with bond lengths ranging from 2.62 to 3.57 Å. Notably, one electrostatic interaction became substantially stronger, contributing −6.05 MolDock score at a distance of 2.62 Å, whereas two other electrostatic contacts exhibited positive energies (+1.04 and +1.26 MolDock score), indicating locally unfavorable or repulsive interactions. Overall, the T state was characterized by fewer hydrogen bonds with favorable geometries, whereas the R2 state exhibited a broader interaction network characterized by stronger electrostatic attraction in some contacts and more diverse hydrogen-bond geometries.

Residue-level energy decomposition further revealed distinct amino acid interaction networks in the two conformations. In the T state, the principal energetic hotspots were Arg141 (−18.19 MolDock score), Thr137 (−17.47), Lys127 (−14.63), Pro95 (−13.86), Lys99 (−7.52), Ser131 (−7.21), Thr134 (−7.08), Phe98 (−6.99), and Ser133 (−6.52 MolDock score). Arg141 contributed through both pairwise interactions (EPair = −14.53 MolDock score) and short-range electrostatic interactions (EElec at distances < 4.5 Å = −2.50 MolDock score), whereas Lys127 exhibited additional long-range electrostatic stabilization (EElec at distances > 4.5 Å = −1.25 MolDock score). Conversely, Asp94, Asp126, and Asp6 made small positive energy contributions, indicating locally unfavorable interactions.

Following the transition to the R2 conformation, Lys99 became the dominant energetic hotspot (−34.31 MolDock score), followed by His103 (−17.88), Ser133 (−13.22), Phe98 (−12.15), Ala130 (−11.94), and Asp126 (−10.69 MolDock score). Asp126 combined favorable van der Waals interactions (EPair = −14.21 MolDock score) with an opposing electrostatic component (EElec = +3.52 MolDock score), whereas Lys99 exhibited the strongest electrostatic interaction observed in either conformation (EElec at distances < 4.5 Å = −6.05 MolDock score). Although residues such as Phe98, Ser133, Thr134, and Pro95 participated in ligand recognition in both conformations, their energetic contributions changed markedly. Heme interactions remained weak in both states (−0.33 to −0.72 MolDock score), indicating that binding was governed primarily by interactions with protein residues.

Per-atom energy decomposition further supported these findings, showing that oxygen atoms dominated polar interactions, whereas carbon atoms contributed mainly through steric contacts. In the T conformation, O4 (−7.62 MolDock score), O3 (−6.91), and O6 (−6.42) were the strongest atomic contributors. O4 exhibited substantial intramolecular strain (EIntra = 2.40 MolDock score) alongside favorable pairwise interactions (EPair = −7.43 MolDock score), long-range electrostatic stabilization (−2.22 MolDock score), and cofactor interaction (−0.37 MolDock score). O1 contributed through both long-range (−1.07) and short-range (−2.50 MolDock score) electrostatic interactions, yielding a total energy of −5.88 MolDock score, whereas O5 exhibited an unfavorable positive total energy (+1.90 MolDock score). Among the carbon atoms, C15, C16, and C23 showed the strongest stabilization, with energies ranging from approximately −6.6 to −6.8 MolDock score.

In the R2 conformation, O1 became the dominant atomic contributor (−9.54 MolDock score), primarily because of enhanced short-range electrostatic interactions (EElec at distances <

[DOI: 10.18502/jabs.v16i4.22275]
Downloaded from jabs.fums.ac.ir at 7:25 +0330 on Sunday November 29th 2026

4.5 Å = −6.05 MolDock score), while O2 (−6.68) and O6 (−7.31 MolDock score) also contributed substantially. Conversely, O4 exhibited only a marginal total energy (−0.07 MolDock score), as favorable long-range electrostatic interactions (−3.77 MolDock score) were offset by unfavorable short-range electrostatic interactions (+2.30 MolDock score) and intramolecular strain (EIntra = 1.80 MolDock score). O7 also exhibited an unfavorable positive contribution (+2.10 MolDock score). Carbon atoms C9, C10, C11, C14, and C25 became more strongly stabilized, with energies ranging from approximately −7.0 to −7.6 MolDock score, indicating enhanced hydrophobic complementarity within the relaxed binding pocket.

Collectively, these results demonstrate that the T conformation favors a more localized hydrogen-bonding network centered on Arg141, Thr137, and Lys127, whereas the R2 conformation redistributes ligand interactions toward Lys99, His103, and Asp126, accompanied by stronger oxygen-centered electrostatic interactions and broader carbon-mediated hydrophobic contacts. This redistribution provides a more favorable predicted interaction landscape, consistent with the superior predicted docking affinity of rosmarinic acid for the relaxed HbS conformation.

The predicted improvement in binding in the R2 conformation was associated with stronger external ligand interactions and more favorable protein-ligand interaction energies, suggesting enhanced stabilization of rosmarinic acid within the R2 binding environment. The more favorable predicted R2 profile was also associated with improved steric complementarity and hydrogen-bonding interactions, including substantial improvements in protein-ligand pairwise (PLP) steric contributions and hydrogen-bond networks. Both short-range and long-range electrostatic interactions were also predicted to be more favorable in the R2 state. Although the internal ligand interaction energy increased slightly, rosmarinic acid exhibited lower predicted torsional strain in R2, suggesting a comparatively more relaxed ligand conformation upon binding. Importantly, despite the more favorable MolDock score in R2, the rerank score was less favorable than that in the T state, highlighting the importance of considering multiple scoring components rather than relying on a single docking descriptor. Overall, the superior predicted binding profile of rosmarinic acid in the R2 conformation appears to be driven primarily by stronger protein-ligand interactions and reduced torsional strain, suggesting that the relaxed HbS conformation provides a more favorable molecular environment for rosmarinic acid than the T conformation (Table 2; Supplementary Appendices 3 and 4).

Comparative Analysis of Curcumin Interactions with Tense and R2 Conformations of HbS

Curcumin exhibited substantial differences in atomic, hydrogen-bonding, and residue-level interaction patterns between the T (tense) and R2 (relaxed) conformations of HbS, indicating pronounced reorganization of the binding environment during the transition from T to R2. Per-atom energy decomposition revealed that oxygen atoms primarily mediated polar interactions, whereas carbon atoms contributed mainly through pairwise steric interactions, including van der Waals contacts. In the T conformation, O4 was the dominant oxygen contributor (−7.31 MolDock score), followed by O0 (−5.40) and O5 (−4.44). O2 and O5 exhibited relatively high intramolecular strain (EIntra = 1.85 and 1.42 MolDock score, respectively), whereas O0 and O4 exhibited lower strain (<1 MolDock score), indicating more favorable energetic contributions. Among the carbon atoms, C15 (−8.22), C23 (−7.66), C19 (−7.61), C9 (−7.46), and C22 (−7.45 MolDock score) represented the principal stabilizing centers, whereas C10, C17, and C25 exhibited elevated internal strain (EIntra > 1 MolDock score).

Downloaded from jabs.fums.ac.ir at 7:25 +0330 on Sunday November 29th 2026 [DOI: 10.18502/jabs.v16i4.22275]

Table 2. Binding Energy Comparison for Amino Acid Residues in Hemoglobin (HBS) Binding Site with Rosmarinic Acid: Tense (T) vs. Relaxed (R2) Conformations.

Per-Residue Binding Energy Contributions of the HBS Model (T) Conformation to Rosmarinic Acid Binding								Per-Residue Binding Energy Contributions of the HBS Model (R2) Conformation to Rosmarinic Acid Binding							
Target Atoms: Molecule	Residue	ID	Total	EP-air	EElec (r > 4.5)	EElec (r < 4.5)	EElec	Target Atoms: Molecule	Residue	ID	Total	EPair	EElec (r > 4.5)	EElec (r < 4.5)	EElec
2HBS [A]	Ala	130	-3.25	-3.25				5E83 [A]	Ala	130	-11.94	-11.94			
2HBS [A]	Arg	141	-18.19	-14.53	-1.15	-2.50		5E83 [A]	Asp	94	0.30896	0	0.31		
2HBS [A]	Asp	94	1.14	0	1.14			5E83 [A]	Asp	126	-10.691	-14.21	1.22	2.30	
2HBS [A]	Lys	99	-7.52	-7.16	-0.36			5E83 [A]	His	103	-17.88	-17.53	-0.35		
2HBS [A]	Lys	139	-0.56	0	-0.56			5E83 [A]	Leu	106	-2.47	-2.47			
2HBS [A]	Phe	98	-6.99	-6.99				5E83 [A]	Leu	129	-4.78	-4.78			
2HBS [A]	Pro	95	-13.86	-13.86				5E83 [A]	Lys	99	-34.31	-26.46	-1.79	-6.05	
2HBS [A]	Ser	133	-6.52	-6.52				5E83 [A]	Lys	127	-0.65	0	-0.65		
2HBS [A]	Ser	138	-3.188	-3.19				5E83 [A]	Phe	98	-12.15	-12.15			
2HBS [A]	Thr	134	-7.08	-7.08				5E83 [A]	Pro	95	-7.68	-7.68			
2HBS [A]	Thr	137	-17.47	-17.47				5E83 [A]	Ser	102	-7.74	-7.74			
2HBS [A]	Tyr	140	-5.60	-5.60				5E83 [A]	Ser	133	-13.22	-13.22			
2HBS [A]	Val	96	-2.18	-2.18				5E83 [A]	Thr	134	-7.21	-7.21			
2HBS [C]	Ala	130	-3.22	-3.22				5E83 [A]	Thr	137	-7.58	-7.58			
2HBS [C]	Asp	6	0.66	0	0.66			5E83 [B]	Arg	104	-6.37	-4.78	-1.59		
2HBS [C]	Asp	126	1.12	0	1.12			5E83 [B]	Asn	108	-1.017	-1.017			
2HBS [C]	Leu	2	-1.22	-1.22				5E83 [B]	Glu	101	1.07	-0.16	1.23		
2HBS [C]	Lys	99	-0.67	0	-0.67			5E83 [B]	Leu	105	-5.78	-5.78			
2HBS [C]	Lys	127	-14.63	-13.38	-1.25			5E83 [B]	Tyr	35	-6.28	-6.28			
2HBS [C]	Ser	131	-7.21	-7.21				5E83 [B]	Val	109	-1.39	-1.39			
2HBS [C]	Val	1	-5.43	-5.43				5E83 [C]	Lys	99	-0.96	0	-0.96		
2HBS [D]	Glu	101	0.31	0	0.31			5E83 [C]	Lys	139	-0.32	0	-0.32		
2HBS [D]	Trp	37	-3.92	-3.92				HEM_201 [A]	(cofactor)	0	-0.67	0			-0.67
HEM_153	(cofactor)	0	-0.71	0			-0.72	HEM_201 [B]	(cofactor)	1	-0.37	0			-0.37
HEM_6	(cofactor)	2	-0.33	0			-0.33	HEM_201 [C]	(cofactor)	2	-0.35	0			-0.34
HEM_7	(cofactor)	3	-0.35	0			-0.35								

[DOI: 10.18502/jabs.v16i4.22275]
Downloaded from jabs.fums.ac.ir at 7:25 +0330 on Sunday November 29th 2026

In contrast, the R2 conformation exhibited a redistribution of atomic interactions, with O1 becoming the strongest oxygen contributor (−7.00 MolDock score), followed by O3 (−6.11) and O0 (−5.33), whereas O2 exhibited an unfavorable positive interaction energy (+0.99 MolDock score). Carbon-mediated stabilization became more uniformly distributed, with C21 (−8.71), C12 (−7.77), C25 (−7.39), C17 (−7.34), and C23 (−7.12 MolDock score) making the strongest contributions, while intramolecular energy penalties became negligible. These findings indicate that stabilization in the T state is concentrated around a limited number of oxygen atoms, whereas the R2 state favors more extensive hydrophobic packing through distributed carbon-centered interactions. This pattern is consistent with improved steric complementarity and accommodation of curcumin's extended aromatic scaffold.

Hydrogen-bond analysis further revealed that both conformations formed four hydrogen bonds, although their strengths and geometries differed markedly. In the T conformation, bond ID1 exhibited the most favorable interaction energy (−2.50 MolDock score), a bond length of 2.91 Å, and a donor-hydrogen-acceptor (D-H-A) angle of 155.26°. Bond ID2 contributed −1.99 MolDock score and exhibited the shortest bond length (2.71 Å), although its angle was less favorable (137.78°). Bonds ID0 and ID3 were weaker, with interaction energies of −0.98 and −1.41 MolDock score, respectively. Nevertheless, ID0 exhibited an almost ideal angle of 178.18° despite its longer bond length of 3.40 Å. In the R2 conformation, bond ID3 reached the most favorable interaction energy (−2.50 MolDock score), with a bond length of 2.77 Å and an excellent angle of 172.25°. Bond ID0 contributed −1.68 MolDock score and exhibited the shortest hydrogen bond observed (2.50 Å), together with a highly favorable angle of 170.00°. Conversely, the target-mediated interactions represented by IDs 1 and 2 were substantially weaker, with interaction energies of −0.009 and −1.02 MolDock score, respectively. Bond ID1 also exhibited unfavorable geometry, with an angle of 102.24° and the longest bond length (3.59 Å). Thus, although both conformations maintained four hydrogen bonds, the T state exhibited a relatively balanced network of moderate interactions, whereas the R2 state relied more heavily on two highly optimized ligand-mediated hydrogen bonds characterized by shorter bond lengths and nearly ideal geometries.

Per-residue energy decomposition likewise revealed extensive reorganization of the interaction network. In the T conformation, Lys99 represented the principal energetic hotspot (−26.95 MolDock score), followed by His103 (−13.12), Asp126 (−12.94), Ser133 (−12.22), Ala130 (−11.42), Leu100 (−10.49), Asn108 (−10.37), Phe98 (−10.24), and Ser102 (−9.34 MolDock score). Additional stabilization was provided by Leu129, Phe36, and Thr134, whereas Ser131, Val96, Arg104, Gln131, and Glu101 contributed minimally (<1 MolDock score). Following the transition to the R2 state, the interaction landscape shifted substantially toward Gly136 (−19.53 MolDock score), Leu81 (−15.52), Leu78 (−13.56), Asn139 (−12.85), Val1 (−11.28), Ala135 (−10.57), and His2 (−10.48). Moderate contributions were observed for Lys132 (−8.74), Val133 (−8.17), Leu3 (−7.10), and His146 (−6.23 MolDock score), whereas Tyr145, Lys82, Ala140, His143, Asp79, Asn80, Val137, and Gln131 contributed only weakly. Gln131 remained a minor contributor in both conformations, with interaction energies of approximately −0.45 to −0.50 MolDock score, whereas the dominant T-state residues, particularly Lys99 and His103, no longer governed ligand binding in the R2 state.

Collectively, these results demonstrate that curcumin adopts distinct binding modes in the two allosteric states of HbS. The T conformation relies on a limited number of localized energetic hotspots and a relatively balanced hydrogen-

[DOI: 10.18502/jabs.v16i4.22275]
Downloaded from jabs.fums.ac.ir at 7:25 +0330 on Sunday November 29th 2026

bonding network, whereas the R2 conformation redistributes stabilization across broader hydrophobic, carbon-centered interactions, highly optimized ligand-mediated hydrogen bonds, and a more diverse network of residue-level interactions. This redistribution provides a more favorable binding environment, consistent with the enhanced predicted docking affinity of curcumin for the relaxed HbS conformation (Table 3; Supplementary Appendices 5 and 6).

The R2 conformation exhibited a more favorable total binding energy than the T conformation, suggesting a stronger predicted binding affinity for the relaxed state. External ligand interactions and protein-ligand interaction energies were also slightly more favorable in R2, which was attributed to improved steric complementarity. Although hydrogen-bonding interactions were more favorable in the T conformation, the internal ligand energy decreased substantially in R2, indicating a more favorable internal energetic state upon binding. Torsional strain increased in the R2 state, suggesting greater rotational adjustments despite the lower internal energy. Furthermore, although the rerank score showed only a modest difference favoring the T state, the overall analysis suggests that curcumin binds more favorably to the R2 conformation because of improved steric compatibility and reduced internal ligand energy, despite the advantages of the T conformation in hydrogen bonding. These findings suggest that the relaxed state of HbS provides a more favorable environment for curcumin accommodation, enhancing protein-ligand interactions while maintaining favorable hydrogen-bonding contributions.

Table 3. Binding Energy Comparison for Amino Acid Residues in Hemoglobin (HBS) Binding Site with Curcumin: Tense (T) vs. Relaxed (R2) Conformations.

Per-Residue Binding Energy Contributions of the HBS Model (T) Conformation to Curcumin Binding					Per-Residue Binding Energy Contributions of the HBS Model (R2) Conformation to Curcumin Binding				
Target Atoms: Molecule	*Residue*	*ID*	*Total*	*EPair*	*Target Atoms: Molecule*	*Residue*	*ID*	*Total*	*EPair*
2HBS [C]	Ala	130	-11.42	-11.42	5E83 [B]	His	146	-6.23	-6.23
2HBS [C]	Asp	126	-12.94	-12.94	5E83 [B]	Tyr	145	-4.64	-4.64
2HBS [C]	His	103	-13.12	-13.12	5E83 [D]	Ala	135	-10.57	-10.57
2HBS [C]	Leu	100	-10.49	-10.49	5E83 [D]	Ala	140	-4.80	-4.80
2HBS [C]	Leu	106	-1.04	-1.04	5E83 [D]	Asn	80	-2.08	-2.08
2HBS [C]	Leu	129	-6.67	-6.67	5E83 [D]	Asn	139	-12.85	-12.85
2HBS [C]	Lys	99	-26.95	-26.95	5E83 [D]	Asp	79	-2.78	-2.78
2HBS [C]	Phe	36	-6.10	-6.10	5E83 [D]	Gln	131	-0.45	-0.45
2HBS [C]	Phe	98	-10.24	-10.24	5E83 [D]	Gly	136	-19.53	-19.53
2HBS [C]	Pro	95	-0.80	-0.80	5E83 [D]	His	2	-10.48	-10.48
2HBS [C]	Ser	102	-9.34	-9.34	5E83 [D]	His	143	-3.27	-3.27
2HBS [C]	Ser	131	-0.45	-0.45	5E83 [D]	Leu	3	-7.10	-7.10
2HBS [C]	Ser	133	-12.22	-12.22	5E83 [D]	Leu	78	-13.56	-13.56
2HBS [C]	Thr	134	-5.76	-5.76	5E83 [D]	Leu	81	-15.52	-15.52
2HBS [C]	Thr	137	-2.36	-2.36	5E83 [D]	Lys	82	-4.42	-4.42
2HBS [C]	Val	96	-0.37	-0.37	5E83 [D]	Lys	132	-8.74	-8.74
2HBS [D]	Arg	104	-0.79	-0.79	5E83 [D]	Val	1	-11.28	-11.28
2HBS [D]	Asn	108	-10.37	-10.37	5E83 [D]	Val	133	-8.17	-8.167
2HBS [D]	Gln	131	-0.50	-0.50	5E83 [D]	Val	137	-1.30	-1.27
2HBS [D]	Glu	101	-0.41	-0.41					
2HBS [D]	Tyr	35	-3.55	-3.55					

[DOI: 10.18502/jabs.v16i4.22275]
Downloaded from jabs.fums.ac.ir at 7:25 +0330 on Sunday November 29th 2026

Comparative Analysis of Voxelotor Interactions with Tense and R2 Conformations of HbS

Comparative analysis of voxelotor binding to the HbS model revealed extensive reorganization of the ligand-binding energy landscape during the structural transition from the T (tense) to the R2 (relaxed) conformation, with substantial changes at the atomic, hydrogen-bonding, and residue-interaction levels. Per-atom energy decomposition revealed a pronounced redistribution of energetic contributions throughout the ligand, indicating that the conformational transition substantially altered the relative contributions of individual atoms to stabilization of the protein-ligand complex.

Among the oxygen atoms, O0 exhibited enhanced stabilization in the R2 conformation, with its total binding energy becoming more favorable, changing from −2.1737 to −3.90967 MolDock score. This improvement was attributable to stronger intermolecular pairwise interactions, as reflected by the change in EPair from −2.44154 to −3.85940 MolDock score, together with a favorable shift in the intramolecular energy component (EIntra) from +0.267834 to −0.0502688 MolDock score. In contrast, O1 exhibited a substantial reduction in its stabilizing contribution, with its total binding energy becoming less favorable, changing from −6.43262 to −2.09125 MolDock score. This change was primarily attributable to a weakening of EPair from −9.10848 to −4.85409 MolDock score, despite nearly unchanged EIntra values of +2.67586 and +2.76284 MolDock score in the T and R2 conformations, respectively.

Similarly, O2 became less energetically favorable, with its total binding energy changing from −7.88244 to −5.35072 MolDock score as EPair decreased in magnitude from −9.38851 to −7.59354 MolDock score. However, O2 uniquely established an additional ligand-cofactor interaction in the R2 conformation, as indicated by an EPair (cofactor) value of −0.176522 MolDock score, suggesting the emergence of an additional interaction pathway following structural relaxation.

Nitrogen atoms generally exhibited greater stabilization in the T conformation. The total binding energy contribution of N3 became less favorable, changing from −6.56213 to −2.74995 MolDock score, whereas N4 maintained nearly identical energetic contributions in the two conformational states (−2.63228 and −2.80130 MolDock score, respectively). N5 underwent one of the most pronounced reductions in stabilization, with its contribution changing from −9.11250 to −3.58120 MolDock score.

Carbon atoms displayed a heterogeneous energetic response to the conformational transition, with several atoms contributing substantially more to stabilization in the R2 state. These included C9, whose total binding energy changed from +3.19398 to −6.57590 MolDock score; C15, from −1.64145 to −7.69754 MolDock score; C16, from −5.35961 to −7.22696 MolDock score; C17, from −5.75453 to −6.96990 MolDock score; C18, from −3.13301 to −6.65486 MolDock score; C19, from −5.11259 to −8.39450 MolDock score; C20, from −1.21834 to −3.96647 MolDock score; C21, from −3.87875 to −7.15089 MolDock score; C22, from −1.99591 to −5.66143 MolDock score; and C23, from −3.66801 to −6.70796 MolDock score. These changes indicate that the corresponding carbon centers became increasingly involved in favorable intermolecular interactions following relaxation of the HbS structure.

Conversely, several carbon atoms exhibited stronger stabilization in the T conformation, including C6 (−6.42433 versus −2.95118 MolDock score), C7 (−7.44063 versus −4.05213 MolDock score), C8 (−6.60094 versus −3.14098 MolDock score), C10 (−8.01796 versus −2.61381 MolDock score), C12 (−6.27960 versus −5.39963 MolDock score), and C24 (−5.42485 versus −1.89234 MolDock score). These differences indicate that the energetic contributions of these

[DOI: 10.18502/jabs.v16i4.22275]
Downloaded from jabs.fums.ac.ir at 7:25 +0330 on Sunday November 29th 2026

atoms were diminished following the transition to the relaxed state.

By comparison, C11, C13, and C14 exhibited relatively modest energetic variations between the two conformations. Their total binding energies were −4.28048 and −5.74416 MolDock score for C11, −3.55316 and −5.04027 MolDock score for C13, and −3.92284 and −6.32392 MolDock score for C14 in the T and R2 conformations, respectively. These findings suggest that these atoms maintained comparatively stable contributions to ligand binding despite the extensive energetic redistribution accompanying the T-to-R2 transition.

Overall, EPair dominated the energetic profile, whereas EIntra primarily served as a compensatory component. Hydrogen-bond analysis further revealed substantial differences between the two conformations. The T conformation formed seven hydrogen bonds, whereas only three were detected in the R2 state. In the T conformation, five interactions were target-donated (IDs 0, 2, 3, 5, and 6), whereas two were ligand-donated (IDs 1 and 4). Bonds 4 and 6 exhibited the most favorable interaction energy (−2.500 MolDock score), with bond lengths of 2.88895 and 2.99306 Å and D-H-acceptor angles of 171.889° and 168.036°, respectively. Bond 0 contributed −2.26788 MolDock score, with a bond length of 2.59915 Å and an angle of 144.583°, whereas bond 2 contributed −1.86070 MolDock score and had a bond length of 2.85743 Å. Bonds 1 (−1.09444 MolDock score), 5 (−0.57531 MolDock score), and 3 (−0.51909 MolDock score) were weaker. Bond 3 had a bond length of 2.46377 Å and an angle of 112.822°.

In the R2 conformation, only three hydrogen bonds were detected, comprising two ligand-donated interactions (IDs 0 and 1) and one target-donated interaction (ID 2). Bond 1 reached −2.500 MolDock score, with a bond length of 2.89656 Å and an angle of 167.450°, whereas bond 0 exhibited an interaction energy of −2.49737 MolDock score, a bond length of 2.59968 Å, and an angle of 179.867°, making it the most linear hydrogen bond observed in either conformation. Bond 2 was considerably weaker (−0.27170 MolDock score), with a bond length of 3.40088 Å and an angle of 106.374°. Thus, although the number of hydrogen bonds decreased markedly in the R2 state, the remaining interactions exhibited highly favorable geometries, particularly those involving the ligand as the hydrogen-bond donor.

Per-residue energy decomposition likewise revealed profound reorganization of the interaction network, with the Total and EPair values identical for every residue. In the T conformation, voxelotor interacted with 13 residues exclusively in chain D of the HbS model (PDB ID: 2HBS). The interaction network was dominated by Asp79 (−18.6012 MolDock score), followed by Val1 (−16.8049), Leu3 (−14.1115), Leu81 (−13.2845), Lys82 (−12.3095), His2 (−12.1137), Asn80 (−9.57989), Leu78 (−7.14572), Lys8 (−6.58830), Gly136 (−5.51531), Asn139 (−2.27176), Ala140 (−2.12316), and Gly83 (−0.580165 MolDock score).

In contrast, the R2 conformation expanded the interaction network to 20 residue entries across chains B, C, and D of the HbS model (PDB ID: 5E83), with Arg104 emerging as the strongest energetic hotspot (−22.2878 MolDock score). Other major contributors included Asn139 (−18.9567), Ala135 (−18.7225), Ala138 (−12.4650), Val134 (−9.78260), Phe103 (−9.16246), Asn108 (−8.62202), and Tyr145 (−8.19327 MolDock score). Additional contributions were observed for Pro100 in chain D (−4.90461), Gln131 (−4.13849), Ala142 (−2.32361), Pro100 in chain B (−2.28884), Gly107 (−1.86024), His146 in chains D and B (−1.74495 and −1.37477, respectively), Glu101 (−0.856747), Gly136 (−0.587989), Phe36 (−0.580092), Leu106 (−0.552010), and Leu105 (−0.532143 MolDock score). Notably, Asn139 was the only residue identified in both conformations, and its contribution increased

[DOI: 10.18502/jabs.v16i4.22275]
Downloaded from jabs.fums.ac.ir at 7:25 +0330 on Sunday November 29th 2026

substantially in magnitude from −2.27176 to −18.9567 MolDock score.

Collectively, these findings demonstrate that voxelotor undergoes extensive energetic redistribution from predominantly polar, oxygen- and nitrogen-centered stabilization in the T conformation toward enhanced carbon-centered hydrophobic and aromatic interactions and a more broadly distributed residue-interaction network in the R2 state. This reorganization is accompanied by a reduction in the number of hydrogen bonds, although the remaining ligand-centered hydrogen bonds retain highly favorable geometries. The findings also indicate the establishment of a broader and more diverse binding interface in the R2 conformation (Table 4; Supplementary Appendices 7 and 8).

The energetic analysis of voxelotor binding to the HbS model revealed a more favorable predicted binding profile in the R2 (relaxed) conformation than in the T (tense) conformation. Key energetic parameters indicated stronger protein-ligand interactions in R2, with the total binding energy and rerank score reflecting substantial improvements. The more favorable predicted binding profile in R2 was associated with stronger external interactions and greater steric contributions, particularly those arising from van der Waals interactions and shape complementarity. Although hydrogen-bonding contributions diminished in R2, this reduction was offset by enhanced steric and hydrophobic interactions, together with lower ligand torsional strain. Consequently, the predicted binding mechanism appears to shift from one characterized by a greater contribution from hydrogen bonding in the T state toward a more sterically optimized interaction pattern in R2, potentially explaining the more favorable predicted binding profile in the relaxed conformation.

Table 4. Binding Energy Comparison for Amino Acid Residues in Hemoglobin (HBS) Binding Site with Voxelotor: Tense (T) vs. Relaxed (R2) Conformations.

Per-Residue Binding Energy Contributions of the HBS Model (T) Conformation to Voxelotor Binding					Per-Residue Binding Energy Contributions of the HBS Model (R2) Conformation to Voxelotor Binding				
Target Atoms: Molecule	Residue	ID	Total	EPair	Target Atoms: Molecule	Residue	ID	Total	EPair
2HBS [D]	Ala	140	-2.12	-2.12	5E83 [B]	His	146	-1.37	-1.37
2HBS [D]	Asn	80	-9.58	-9.60	5E83 [B]	Pro	100	-2.29	-2.29
2HBS [D]	Asn	139	-2.27	-2.27	5E83 [B]	Tyr	145	-8.19	-8.19
2HBS [D]	Asp	79	-18.60	-18.60	5E83 [C]	Phe	36	-0.58	-0.58
2HBS [D]	Gly	83	-0.58	-0.58	5E83 [D]	Ala	135	-18.72	-18.72
2HBS [D]	Gly	136	-5.52	-5.52	5E83 [D]	Ala	138	-12.47	-12.47
2HBS [D]	His	2	-12.11	-12.11	5E83 [D]	Ala	142	-2.32	-2.32
2HBS [D]	Leu	3	-14.11	-14.11	5E83 [D]	Arg	104	-22.29	-22.29
2HBS [D]	Leu	78	-7.15	-7.15	5E83 [D]	Asn	108	-8.62	-8.62
2HBS [D]	Leu	81	-13.28	-13.28	5E83 [D]	Asn	139	-18.96	-18.96
2HBS [D]	Lys	8	-6.59	-6.59	5E83 [D]	Gln	131	-4.14	-4.14
2HBS [D]	Lys	82	-12.31	-12.31	5E83 [D]	Glu	101	-0.86	-0.86
2HBS [D]	Val	1	-16.80	-16.80	5E83 [D]	Gly	107	-1.86	-1.86
					5E83 [D]	Gly	136	-0.587989	-0.59
					5E83 [D]	His	146	-1.74495	-1.74
					5E83 [D]	Leu	105	-0.532143	-0.53
					5E83 [D]	Leu	106	-0.55201	-0.55
					5E83 [D]	Phe	103	-9.16246	-9.16
					5E83 [D]	Pro	100	-4.90461	-4.90
					5E83 [D]	Val	134	-9.7826	-9.78

[DOI: 10.18502/jabs.v16i4.22275]
Downloaded from jabs.fums.ac.ir at 7:25 +0330 on Sunday November 29th 2026

Comparative Analysis of CID:162739375 Interactions with Tense and R2 Conformations of HbS

Comparative analysis of hydrogen-bonding and residue-level interactions revealed substantial remodeling of the binding mechanism of CID 162739375 during the transition of the HbS model from the T (tense) to the R2 (relaxed) conformation, while the principal energetic hotspot remained conserved. Hydrogen-bond analysis revealed that the ligand formed seven hydrogen bonds in the T conformation and six in the R2 conformation, indicating a slight reduction in the number of interactions following the conformational transition. In the T state, the hydrogen-bonding network comprised four ligand-donated interactions (IDs 0, 2, 3, and 6) and three target-donated interactions (IDs 1, 4, and 5). The strongest interactions were bonds 0 and 3, each exhibiting the maximum hydrogen-bond energy of −2.500 MolDock score. Bond 0 had a bond length of 2.65071 Å and a nearly linear D-H-acceptor angle of 175.188° (100%), whereas bond 3 had a bond length of 2.64352 Å and a D-H-acceptor angle of 154.976° (100%). Bond 2 also contributed substantially to stabilization (−2.38855 MolDock score; 2.92891 Å; 147.325°, 95.54%), whereas bond 6 provided moderate stabilization (−1.02975 MolDock score; 3.05252 Å; 115.405°, 42.34%). Target-donated bonds were considerably weaker, including bond 4 (−0.76851 MolDock score; 2.87050 Å; 108.444°, 30.74%), bond 5 (−0.04512 MolDock score), which nevertheless exhibited a favorable orientation (165.994°, 100%), and bond 1 (−0.00018 MolDock score; AA-A-D angle of 90.036°, 0.36%; D-H-acceptor angle of 97.016°, 11.69%), indicating negligible stabilization.

In the R2 conformation, six hydrogen bonds were identified, comprising three ligand-donated interactions (IDs 0, 2, and 4) and three interactions in which either the ligand or the target could act as the donor (IDs 1, 3, and 5), suggesting greater flexibility in hydrogen-bond donor assignment. Bonds 0 and 2 again reached the maximum interaction energy (−2.500 MolDock score). Bond 0 had a bond length of 3.01374 Å and a D-H-acceptor angle of 176.478° (100%), whereas bond 2 had a bond length of 2.63329 Å and an angle of 173.791° (100%). Bond 5 also remained strong (−2.29267 MolDock score; 3.08027 Å; 145.024°, 91.71%), whereas bond 4 contributed −1.22847 MolDock score (3.35431 Å; 174.191°, 100%). The remaining interactions were weaker, including bond 1 (−0.38442 MolDock score; 3.52312 Å; 164.278°, 100%) and bond 3 (−0.17132 MolDock score; 3.32389 Å; 101.886°, 19.81%). Overall, the T conformation supported a slightly larger hydrogen-bonding network with more clearly differentiated ligand-donated and target-donated interactions, whereas the R2 conformation retained the strongest hydrogen bonds while exhibiting greater flexibility in donor assignment and maintaining favorable geometries for several interactions.

Per-residue energy decomposition further demonstrated substantial remodeling of the interaction landscape, with Total and EPair values remaining identical for every residue, indicating that intermolecular pairwise interactions accounted for the reported residue-level interaction energies. In the T conformation, 17 residues contributed favorably, primarily in chain C of the HbS model (PDB ID: 2HBS), with Tyr35 being the only contributing residue from chain D. Lys99 constituted the principal energetic hotspot (−24.1556 MolDock score), followed by Ser133 (−13.3599), Phe98 (−12.0522), Pro95 (−11.3326), Ala130 (−11.3209), Asp126 (−10.5759), Leu129 (−9.54282), Ser102 (−9.30264), Thr134 (−9.02575), Thr137 (−7.22207), and His103 (−6.31120 MolDock score). The remaining residues made smaller contributions: Leu106 (−2.32904 MolDock score), Val96 (−1.56592), Asn97 (−0.40840), Leu100 (−0.35313), Leu125 (−0.33343), and Tyr35 (−0.30548).

The R2 conformation expanded the interaction network to 20 residues across chains C and D

[DOI: 10.18502/jabs.v16i4.22275]
Downloaded from jabs.fums.ac.ir at 7:25 +0330 on Sunday November 29th 2026

of the HbS model (PDB ID: 5E83). Lys99 remained the dominant hotspot, with slightly stronger stabilization (−24.6576 MolDock score), whereas His103 exhibited the largest increase in energetic contribution (−17.6910 MolDock score), becoming the second strongest contributor. Additional major interactions involved Asp126 (−13.5519 MolDock score), Ala130 (−12.2849), Phe98 (−11.0732), Tyr35 (−9.74322), Ser133 (−9.68966), Pro95 (−8.52291), Asn108 (−7.88119), Thr134 (−7.32582), Leu105 (−4.94461), Ser102 (−4.42755), Val109 (−4.38041), Leu129 (−3.86752), Leu106 (−3.30971), Thr137 (−2.32806), His122 (−2.14879), Arg104 (−1.94484), Cys112 (−1.92956), and Ser131 (−0.36588 MolDock score). Comparison of the two conformations confirmed that Lys99 remained the principal energetic hotspot, with its contribution changing from −24.1556 to −24.6576 MolDock score, whereas His103 (from −6.31120 to −17.6910), Asp126 (from −10.5759 to −13.5519), and Ala130 (from −11.3209 to −12.2849) exhibited substantially stronger contributions in R2.

Conversely, the contributions of Ser133 (from −13.3599 to −9.68966 MolDock score), Leu129 (from −9.54282 to −3.86752), Ser102 (from −9.30264 to −4.42755), Thr137 (from −7.22207 to −2.32806), and Pro95 (from −11.3326 to −8.52291) became less favorable, whereas Phe98 and Thr134 remained relatively stable. The recruitment of His122, Ser131, Arg104, Asn108, Cys112, Leu105, and Val109, together with the pronounced increase in the contribution of Tyr35 (from −0.30548 to −9.74322 MolDock score), indicates that the T-to-R2 transition broadens the interaction interface. This reorganization enables CID 162739375 to engage a more diverse network of charged, polar, aromatic,

Table 5. Binding Energy Comparison for Amino Acid Residues in Hemoglobin (HBS) Binding Site with CID 162739375: Tense (T) vs. Relaxed (R2) Conformations.

Per-Residue Binding Energy Contributions of the HBS Model (T) Conformation to CID Number: 162739375 Binding					Per-Residue Binding Energy Contributions of the HBS Model (R2) Conformation to CID Number: 162739375 Binding				
Target Atoms: Molecule	Residue	ID	Total	EPair	Target Atoms: Molecule	Residue	ID	Total	EPair
2HBS [C]	Ala	130	-11.32	-11.32	5E83 [C]	Ala	130	-12.28	-12.28
2HBS [C]	Asn	97	-0.41	-0.41	5E83 [C]	Asp	126	-13.55	-13.55
2HBS [C]	Asp	126	-10.58	-10.58	5E83 [C]	His	103	-17.69	-17.69
2HBS [C]	His	103	-6.31	-6.31	5E83 [C]	His	122	-2.149	-2.15
2HBS [C]	Leu	100	-0.35	-0.35	5E83 [C]	Leu	106	-3.31	-3.31
2HBS [C]	Leu	106	-2.33	-2.33	5E83 [C]	Leu	129	-3.87	-3.87
2HBS [C]	Leu	125	-0.33	-0.33	5E83 [C]	Lys	99	-24.66	-24.66
2HBS [C]	Leu	129	-9.54	-9.54	5E83 [C]	Phe	98	-11.07	-11.07
2HBS [C]	Lys	99	-24.16	-24.16	5E83 [C]	Pro	95	-8.52	-8.52
2HBS [C]	Phe	98	-12.05	-12.05	5E83 [C]	Ser	102	-4.43	-4.43
2HBS [C]	Pro	95	-11.33	-11.33	5E83 [C]	Ser	131	-0.37	-0.37
2HBS [C]	Ser	102	-9.30	-9.30	5E83 [C]	Ser	133	-9.70	-9.69
2HBS [C]	Ser	133	-13.36	-13.36	5E83 [C]	Thr	134	-7.33	-7.33
2HBS [C]	Thr	134	-9.02	-9.026	5E83 [C]	Thr	137	-2.33	-2.33
2HBS [C]	Thr	137	-7.22	-7.22	5E83 [D]	Arg	104	-1.94	-1.94
2HBS [C]	Val	96	-1.57	-1.57	5E83 [D]	Asn	108	-7.88	-7.88
2HBS [D]	Tyr	35	-0.31	-0.31	5E83 [D]	Cys	112	-1.93	-1.93
					5E83 [D]	Leu	105	-4.94	-4.94
					5E83 [D]	Tyr	35	-9.74	-9.74
					5E83 [D]	Val	109	-4.38	-4.38041

[DOI: 10.18502/jabs.v16i4.22275]
Downloaded from jabs.fums.ac.ir at 7:25 +0330 on Sunday November 29th 2026

and hydrophobic residues while preserving the dominant contribution of Lys99 and maintaining a substantial hydrogen-bonding network (Table 5; Supplementary Appendices 9 and 10).

Taken together, the energetic analysis of CID 162739375 binding to the HbS model indicates that most ligand atoms contributed favorably to stabilization, with intermolecular pairwise interactions representing the principal energetic component and intramolecular energy generally providing smaller compensatory contributions. Certain oxygen and carbon atoms made particularly substantial stabilizing contributions, although some atoms also exhibited unfavorable internal energy components. Hydrogen-bond analysis confirmed substantial interaction networks in both the T and R2 conformations, with a slight reduction in the number of hydrogen bonds following the conformational transition. Although the T conformation supported a greater number of hydrogen bonds, the R2 state permitted greater flexibility in interactions involving alternative donor assignments. Overall, these findings suggest that CID 162739375 is stabilized through a combination of interaction mechanisms in both conformational states and support its predicted binding affinity for HbS.

Comparative Analysis of CID:24015539 Interactions with Tense and R2 Conformations of HbS

Per-atom energy decomposition demonstrated that every atom had a negative total binding energy in both conformational states, indicating favorable overall energetic contributions at the atomic level. Intermolecular pairwise interaction energy (EPair) represented the principal component of ligand binding, whereas the intramolecular energy component (EIntra) predominantly served as a compensatory term. In the T conformation, oxygen atoms made the most prominent stabilizing contributions, with O1 exhibiting the strongest contribution (MolDock score = −10.8542; EPair = −10.5171; EIntra = −0.33717), followed by O2 (MolDock score = −7.08717) and O4 (MolDock score = −6.01458). Upon transition to the R2 conformation, the stabilizing contributions of O1, O2, O4, and O0 became less favorable, with MolDock scores of −7.09894, −5.92948, −4.19003, and −2.00504, respectively, indicating reduced energetic contributions from these atoms within the binding interface.

In contrast, O3 exhibited enhanced stabilization during the conformational transition, with its MolDock score becoming more favorable, changing from −5.52144 to −6.32534. This improvement was primarily attributable to stronger intermolecular pairwise interactions, as reflected by the change in EPair from −5.30269 to −7.68493. Carbon atoms exhibited a distinct energetic response, with several making substantially greater stabilizing contributions in the R2 conformation than in the T state. These included C8 (MolDock score: from −3.28344 to −10.2509), C6 (from −0.71595 to −7.31057), C7 (from −4.62670 to −8.04553), C12 (from −7.78303 to −8.15285), C18 (from −4.18688 to −7.14565), C15 (from −2.05123 to −6.00103), and C5 (from −6.05451 to −6.15233). These findings indicate that these carbon centers became more strongly involved in favorable intermolecular interactions following the conformational transition.

Conversely, several carbon atoms exhibited diminished stabilizing contributions in the R2 conformation, including C11 (MolDock score: from −8.68791 to −5.73299), C16 (from −4.94030 to −3.28117), C17 (from −3.79864 to −3.46138), C19 (from −4.85907 to −4.14618), and C9 (from −5.58643 to −3.30879). These changes indicate that the energetic contributions of these atoms became less favorable following structural relaxation. C13 also exhibited a less favorable contribution, with its MolDock score changing from −7.82822 to −5.89578.

Analysis of the intramolecular energy component further revealed that most atoms exhibited positive EIntra values in the R2

[DOI: 10.18502/jabs.v16i4.22275]
Downloaded from jabs.fums.ac.ir at 7:25 +0330 on Sunday November 29th 2026

conformation, reflecting increased ligand conformational strain associated with accommodation within the relaxed binding environment. Nevertheless, C8 (EIntra = −1.34676 MolDock score) and C12 (EIntra = −1.46149 MolDock score) remained notable exceptions, retaining favorable intramolecular contributions despite the overall increase in conformational strain. These findings suggest that these atoms helped maintain local structural stability while supporting enhanced intermolecular interactions in the R2 state.

Hydrogen-bond analysis further revealed that an extensive interaction network was maintained in both conformations, comprising seven hydrogen bonds in the T conformation and six in the R2 conformation. The T state contained three ligand-donated interactions (IDs 0, 3, and 6), three target-donated interactions (IDs 1, 2, and 4), and one interaction in which either the ligand or the target could serve as the donor (ID 5). Bonds 0, 3, and 5 exhibited the maximum interaction energy (−2.500 MolDock score) and nearly ideal geometries, with bond lengths and angles of 2.75850 Å and 179.211°, 2.82435 Å and 177.867°, and 2.79728 Å and 178.133°, respectively. Additional interactions included bond 2 (−2.30746 MolDock score; 2.91097 Å; 164.542°), bond 4 (−1.60562 MolDock score; 3.05501 Å; 128.535°), bond 6 (−1.34075 MolDock score; 3.22125 Å; 132.479°), and bond 1 (−0.63576 MolDock score; 2.80696 Å; 105.258°).

The R2 conformation comprised one ligand-donated interaction (ID 3), two target-donated interactions (IDs 0 and 5), and three interactions involving alternative donor assignments (IDs 1, 2, and 4). Bonds 4 and 5 retained the maximum interaction energy (−2.500 MolDock score). Bond 1 contributed −1.81323 MolDock score (2.51759 Å; 163.065°), while bond 2 contributed −0.94056 MolDock score (2.41287 Å; 164.117°). Bond 3 exhibited the shortest hydrogen-bond length (2.37176 Å), with an interaction energy of −0.59802 MolDock score and an angle of 155.432°. Bond 0 represented the weakest interaction (−0.26010 MolDock score; 3.47716 Å; 115.409°).

Residue-level energy decomposition also revealed marked reorganization of the binding interface, despite identical Total and EPair values for every residue. The T conformation involved 14 residue entries across chains A, C, and D, with Arg141 in chain A constituting the dominant energetic hotspot (−31.1115 MolDock score). Other contributors included Lys127 (−12.8441 MolDock score), Thr137 (−12.4836), Ser138 (−11.1682), Val1 (−8.56531), Tyr140 (−7.42640), Ser131 (−6.57053), Ala130 (−3.58071), Trp37 (−2.53941), Lys139 (−2.34518), Thr134 in chains C and A (−1.69627 and −1.43064, respectively), Leu2 (−1.23164), and Pro95 (−0.56074 MolDock score).

In the R2 conformation, the interaction network expanded to 17 residue entries across chains C and D, with the principal hotspot shifting to Lys99 (−31.0563 MolDock score). Additional stabilizing contributions were made by His103 (−12.4945 MolDock score), Ala130 (−12.2167), Phe98 (−9.88976), Ser102 (−9.04870), Ser133 (−8.22653), Asn108 (−8.21195), Asp126 (−7.61579), Tyr35 (−7.07061), Leu129 (−5.20155), Leu105 (−4.63992), Pro95 (−4.19914), Arg104 (−3.20140), Thr134 (−2.64525), Leu106 (−2.10035), Leu100 (−0.52764), and Thr137 (−0.31359 MolDock score).

Collectively, these findings demonstrate that, although both conformations maintain a prominent energetic hotspot, the identity of the dominant residue changes from Arg141 in the T state to Lys99 in the R2 state. The T conformation preferentially supports oxygen-centered interactions and highly linear hydrogen bonds, whereas the R2 conformation redistributes stabilization toward carbon-centered interactions and a broader network of charged, polar, aromatic, and hydrophobic residues. This reorganization reflects the adaptation of CID 24015539 to the altered geometry of the relaxed HbS binding pocket.

[DOI: 10.18502/jabs.v16i4.22275]
Downloaded from jabs.fums.ac.ir at 7:25 +0330 on Sunday November 29th 2026

Table 6. Binding Energy Comparison for Amino Acid Residues in Hemoglobin (HBS) Binding Site with CID 24015539: Tense (T) vs. Relaxed (R2) Conformations.

Per-Residue Binding Energy Contributions of the HBS Model (T) Conformation to CID Number: 24015539 Binding					Per-Residue Binding Energy Contributions of the HBS Model (R2) Conformation to CID Number: 24015539 Binding				
Target Atoms: Molecule	Residue	ID	Total	EPair	Target Atoms: Molecule	Residue	ID	Total	EPair
2HBS [A]	Arg	141	-31.11	-31.11	5E83 [C]	Ala	130	-12.22	-12.22
2HBS [A]	Lys	139	-2.35	-2.34	5E83 [C]	Asp	126	-7.62	-7.62
2HBS [A]	Pro	95	-0.56	-0.56	5E83 [C]	His	103	-12.49	-12.49
2HBS [A]	Ser	138	-11.17	-11.17	5E83 [C]	Leu	100	-0.53	-0.53
2HBS [A]	Thr	134	-1.43	-1.43	5E83 [C]	Leu	106	-2.10	-2.10
2HBS [A]	Thr	137	-12.48	-12.48	5E83 [C]	Leu	129	-5.20	-5.20
2HBS [A]	Tyr	140	-7.43	-7.43	5E83 [C]	Lys	99	-31.06	-31.06
2HBS [C]	Ala	130	-3.58	-3.58	5E83 [C]	Phe	98	-9.89	-9.89
2HBS [C]	Leu	2	-1.23	-1.23	5E83 [C]	Pro	95	-4.20	-4.20
2HBS [C]	Lys	127	-12.84	-12.84	5E83 [C]	Ser	102	-9.05	-9.05
2HBS [C]	Ser	131	-6.57	-6.57	5E83 [C]	Ser	133	-8.23	-8.23
2HBS [C]	Thr	134	-1.70	-1.70	5E83 [C]	Thr	134	-2.65	-2.65
2HBS [C]	Val	1	-8.57	-8.57	5E83 [C]	Thr	137	-0.31	-0.31
2HBS [D]	Trp	37	-2.54	-2.54	5E83 [D]	Arg	104	-3.20	-3.20
					5E83 [D]	Asn	108	-8.21	-8.21
					5E83 [D]	Leu	105	-4.64	-4.64
					5E83 [D]	Tyr	35	-7.07	-7.07

Overall, the comparison indicates that the transition from T to R2 substantially redistributes the energetic contributions associated with CID 24015539 binding, with a relative shift toward more favorable carbon-centered interactions while preserving an adaptable hydrogen-bonding network. Changes in hydrogen-bond geometry, donor distribution, and atom-specific energetic contributions collectively demonstrate the complex interplay among polar, hydrophobic, intermolecular, and intramolecular interactions that may influence the predicted binding behavior of CID 24015539 across the two HbS conformational states (Table 6; Supplementary Appendices 11 and 12).

Discussion

Conformational Selectivity and Allosteric Remodeling

The docking results suggest that most of the investigated ligands preferentially bind to the relaxed (R2) conformation of sickle hemoglobin (HbS) rather than the tense (T) state. Rosmarinic acid, curcumin, voxelotor, CID 162739375, CID 141386569, and CID 24015539 exhibited more favorable predicted MolDock scores in the R2 conformation, whereas vanillin showed relatively little conformational dependence. These computational findings are consistent with the Monod-Wyman-Changeux allosteric model and support the hypothesis that conformational transitions in HbS can alter the physicochemical properties of the binding pocket. The R2 conformation differs structurally from the polymerization-prone T state, thereby providing a distinct molecular environment for ligand accommodation and stabilization (30).

Energetic Analysis of Rosmarinic Acid Binding

Among the compounds examined, rosmarinic acid exhibited one of the largest improvements in predicted binding affinity in the R2

[DOI: 10.18502/jabs.v16i4.22275]
Downloaded from jabs.fums.ac.ir at 7:25 +0330 on Sunday November 29th 2026

conformation, with its MolDock score becoming more favorable, changing from −118.84 in the T state to −149.57 in the R2 state. Residue-level energy decomposition revealed a shift in the principal energetic hotspots from Arg141, Thr137, and Lys127 in the T conformation toward Lys99, His103, Asp126, Ser133, Phe98, and Ala130 in the R2 state. Lys99 showed a particularly pronounced increase in its energetic contribution, becoming the dominant contributor (−34.31 MolDock score) and exhibiting the strongest short-range electrostatic interaction (EElec at distances < 4.5 Å = −6.05 MolDock score).

Per-atom energy decomposition provided further mechanistic insight. Oxygen atom O1 became substantially more favorable because of enhanced short-range electrostatic interactions, while aromatic carbon atoms C9, C10, C11, C14, and C25 exhibited stronger pairwise interactions. These findings suggest that the more favorable predicted binding profile of rosmarinic acid in the R2 state is associated with the combined contributions of enhanced oxygen-centered polar interactions and aromatic carbon-mediated hydrophobic contacts (30).

Curcumin, Voxelotor, and Synthetic Ligands

Curcumin exhibited a similar computational profile, with a more favorable predicted docking score in the R2 conformation and a marked reduction in internal ligand energy, suggesting a more favorable internal energetic state. Although curcumin formed four hydrogen bonds in both conformations, stabilization in the R2 state was concentrated in two ligand-mediated hydrogen bonds with nearly ideal geometries. Several aromatic carbon atoms, including C21, C12, C25, C17, and C23, also exhibited stronger stabilizing contributions, while residue-level interactions shifted toward Gly136, Leu81, Leu78, Asn139, and Ala135.

Voxelotor likewise exhibited a more favorable predicted docking score in the R2 conformation, with binding occurring within the alpha-chain cleft of hemoglobin. Notably, the number of predicted hydrogen bonds decreased from seven in the T state to three in the R2 state; however, the remaining bonds exhibited nearly ideal geometries, suggesting that favorable interaction geometry may partly compensate for the reduction in hydrogen-bond number. CID 162739375 also showed a preference for the R2 state despite an increase in internal ligand energy. Its molecular scaffold may support multiple simultaneous contacts within the binding pocket, allowing favorable intermolecular interactions to outweigh the energetic cost associated with ligand deformation (9, 30).

Unifying Principles and Practical Implications

A broader finding across the investigated compounds is that hydrogen bonding alone does not fully account for differences in predicted docking scores. For example, CID 24015539 exhibited a more favorable overall predicted docking score in the R2 conformation despite a less favorable predicted hydrogen-bond contribution than in the T state. This finding highlights the contributions of steric complementarity, electrostatic interactions, and residue-specific van der Waals contacts to the overall docking score. Consequently, a key implication for rational drug design is that developing novel antisickling agents requires the combined optimization of multiple intermolecular interactions rather than an exclusive focus on individual hydrogen bonds. Overall predicted binding performance is likely to depend on the collective balance of interactions within the conformationally distinct R2 binding environment (9, 30).

Limitations

Despite these promising computational findings, several important limitations and potential sources of error should be acknowledged. First, molecular docking primarily estimates static binding poses and cannot fully account for dynamic thermal fluctuations or the entropic penalties associated with ligand binding under physiological conditions. Second, scoring

[DOI: 10.18502/jabs.v16i4.22275]
Downloaded from jabs.fums.ac.ir at 7:25 +0330 on Sunday November 29th 2026

functions such as MolDock provide relative computational estimates rather than exact quantitative thermodynamic measurements and may therefore yield inaccurate affinity rankings, including false-positive predictions. Third, the current computational model does not explicitly account for solvent effects or water-mediated interaction networks, both of which can influence protein-ligand interactions within the highly solvated hemoglobin binding pocket.

Conclusion

The present computational study suggests that the relaxed R2 conformation of sickle hemoglobin may provide a more favorable molecular environment for the binding of several natural and synthetic ligands than the tense T state. Detailed energetic and atomic decompositions suggest that the more favorable predicted binding profiles of rosmarinic acid, curcumin, voxelotor, and CID 162739375 in the R2 state may be associated with enhanced electrostatic complementarity, broader hydrophobic packing, and changes in residue-specific energetic hotspots, including Lys99. Furthermore, the findings suggest that predicted binding behavior depends on the combined contributions of van der Waals forces and favorable interaction geometries rather than on the number of hydrogen bonds alone.

Overall, these findings support the biophysical hypothesis that selectively stabilizing the relaxed HbS conformation may represent a promising structural strategy for developing new antisickling agents. The conformational adaptability observed for the investigated polyphenolic compounds may also provide useful starting points for future molecular optimization. Further experimental studies are needed to validate these *in silico* findings and assess the potential of these compounds as allosteric modulators for the treatment of sickle cell disease.

Acknowledgments

The authors would like to thank the Department of Biology at Tarbiat Modares University, Tehran, Iran, for providing the academic facilities and support required for this research. The authors also acknowledge Amol University of Special Modern Technologies, Amol, Iran, for its institutional support.

Conflict of Interest

The authors declare that they have no conflicts of interest regarding this study.

Funding

This research was financially supported by Amol University of Special Modern Technologies and Tarbiat Modares University.

Ethical Considerations

Ethical approval was not required for this computational study.

Code of Ethics

The ethics code is IR.MODARES.REC.1401.149. (Tarbiat Modares University)

Authors' Contributions

All authors contributed to the conception and design of the study, analysis and interpretation of the results, and preparation of the manuscript. All authors have read and approved the final version of the manuscript.

Data Availability Statement

The datasets analyzed in this study are available from publicly accessible databases. Protein structures were obtained from the Research Collaboratory for Structural Bioinformatics Protein Data Bank (RCSB PDB), and ligand structures were retrieved from the PubChem database. Additional data supporting the findings of this study are available from the corresponding author upon reasonable request.

[DOI: 10.18502/jabs.v16i4.22275]
Downloaded from jabs.fums.ac.ir at 7:25 +0330 on Sunday November 29th 2026

Artificial Intelligence (AI) Disclosure

Artificial intelligence (AI) tools were used during the preparation of this manuscript to assist with language editing, grammatical correction, and improvements in the clarity and readability of the English text. The authors reviewed and verified all AI-assisted text and remain fully responsible for the accuracy, integrity, and originality of the manuscript and its scientific content.

References

1 Diamantidis MD, Ikonomou G, Argyrakouli I, Pantelidou D, Delicou S. Genetic modifiers of hemoglobin expression from a clinical perspective in hemoglobinopathy patients with beta thalassemia and sickle cell disease. Int J Mol Sci. 2024; 25(22):11886.
2 Yu Y, Lu S, Gao Z, Zheng H, Ke G. Do deep learning models really outperform traditional approaches in molecular docking? arXiv [Preprint]. 2023; arXiv:2302.07134.
3 Triuzzi E, Mengoni R, Micucci F, Bonanni D, Ottaviani D, Beccari AR, et al. Molecular docking via weighted subgraph isomorphism on quantum annealers. Quantum Sci Technol. 2025; 10(4):045049.
4 Suriana P, Dror RO. Enhancing ligand pose sampling for molecular docking. arXiv [Preprint]. 2023; arXiv:2312.00191.
5 Powalski R, Klockiewicz B, Jaśkowski M, Topolski B, Dąbrowski-Tumański P, Wiśniewski M, et al. RapidDock: Unlocking proteome-scale molecular docking. arXiv [Preprint]. 2024; arXiv:2411.00004.
6 Gao S, Serebrennikova L, Murakami R, Boinapally S, Ray S, Pomper MG, et al. Absolute quantitative photoacoustic imaging for contrast agents concentration estimation using a spectral decomposition approach. Mol Imaging. 2025; 24:15353508251368629.
7 Park CM, Nagel RL, Blumberg WE, Peisach J, Magliozzo RS. Sulfhemoglobin. Properties of partially sulfurated tetramers. J Biol Chem. 1986; 261(19):8805-10.
8 Ahmed MH, Ghatge MS, Safo MK. Hemoglobin: structure, function and allostery. Subcell Biochem. 2020; 94:345-82.
9 Harrington DJ, Adachi K, Royer WE Jr. The high resolution crystal structure of deoxyhemoglobin S. J Mol Biol. 1997; 272(3):398-407.
10 de la Cueva Tamanaha M, Cabrera EF, Sargeant J, Gershon PD, Russell PPS, Cocco MJ. Voxelotor (Oxbryta) binds multiple hemoglobin sites and influences protein structure. bioRxiv [Preprint]. 2025; 2025.05.12.653546.
11 Mirchandani AS, Sanchez-Garcia MA, Walmsley SR. How oxygenation shapes immune responses: emerging roles for physioxia and pathological hypoxia. Nat Rev Immunol. 2025; 25(3):161-77.
12 Sadiq IZ, Abubakar FS, Usman HS, Abdullahi AD, Ibrahim B, Kastayal BS, et al. Thalassemia: pathophysiology, diagnosis, and advances in treatment. Thalass Rep. 2024; 14(4):81-102.
13 Nemkov T, Stephenson D, Earley EJ, Keele GR, Hay A, Key A, et al. Biological and genetic determinants of glycolysis: phosphofructokinase isoforms boost energy status of stored red blood cells and transfusion outcomes. Cell Metab. 2024; 36(9):1979-97.e13.
14 Vissa M, Vichinsky E. Voxelotor for the treatment of sickle cell disease. Expert Rev Hematol. 2021; 14(3):253-62.
15 Niesor EJ, Perez A, Bordat C, Lagrissi-Thode F, Nader E, Connes P. Challenges of the allosteric regulation of hemoglobin by interaction with Cys93 of the β chain for the treatment of sickle cell disease. J Sickle Cell Dis. 2025; 2(1):yoaf012.
16 Goodsell DS, Burley SK. RCSB Protein Data Bank resources for structure-facilitated design of mRNA vaccines for existing and emerging viral pathogens. Structure. 2022; 30(1):55-68.e2.
17 Oliveira JMV, da Silva AD, Soares AMDS, de Azevedo WF Jr. Molegro virtual Docker for docking screens. Methods Mol Biol. 2026; 2984:139-52.
18 Bitencourt-Ferreira G, de Azevedo WF Jr. Molegro virtual Docker for docking. Methods Mol Biol. 2019; 2053:149-67.
19 Pooreydy Golaki B, Aminzadeh S, Karkhane AA, et al. Cloning, expression, purification, and characterization of lipase 3646 from thermophilic indigenous Cohnella sp. A01. Protein Expr Purif. 2015; 109:120-6.
20 Yousefi R. Docking study of HIV-1 reverse transcriptase with well-known nucleoside reverse transcriptase inhibitors. J Adv Pharm Res. 2024; 8(3):176-87.
21 Khaleghinejad S, Niri M, Fazilati A, et al. The role of protein engineering in the design and production of recombinant proteins. Int J Vaccines Vaccin. 2016; 3(3):00067.
22 Khaleghinejad SH, Motalleb G, Karkhane AA, Aminzadeh S, Yakhchali B. Study the effect of F17S mutation on the chimeric Bacillus thermocatenulatus lipase. J Genet Eng Biotechnol. 2016; 14(1):83-9.

[DOI: 10.18502/jabs.v16i4.22275]
Downloaded from jabs.fums.ac.ir at 7:25 +0330 on Sunday November 29th 2026

23 Hansel-Harris AT, Tillack AF, Santos-Martins D, Holcomb M, Forli S. Docking guidance with experimental ligand structural density improves docking pose prediction and virtual screening performance. Protein Sci. 2025; 34(3):e70082.
24 Blanes-Mira C, Fernández-Aguado P, de Andrés-López J, Fernández-Carvajal A, Ferrer-Montiel A, Fernández-Ballester G. Comprehensive survey of consensus docking for high-throughput virtual screening. Molecules. 2022; 28(1):175.
25 Dong Y, Rousitanmu R, Zhao Y, Zhang Q, Yu M. Computationally guided rational design of a resveratrol O-methyltransferase with expanded substrate specificity. In: Proceedings of the 2025 6th International Symposium on Artificial Intelligence for Medical Sciences. 2025. p.638-45.
26 Nivatya HK, Singh A, Kumar N, Sonam, Sharma L, Singh V, et al. Assessing molecular docking tools: understanding drug discovery and design. Futur J Pharm Sci. 2025; 11(1):111.
27 Wang X, Li L, Shen X, Lu X. Rational design strategies in DNA-encoded libraries for drug discovery. Angew Chem Int Ed. 2025; 64(34):e202511839.
28 Bitencourt-Ferreira G, de Azevedo WF Jr. Machine learning to predict binding affinity. Methods Mol Biol. 2019; 2053:251-73.
29 Thomsen R, Christensen MH. MolDock: a new technique for high-accuracy molecular docking. J Med Chem. 2006; 49(11):3315-21.
30 Monod J, Wyman J, Changeux JP. On the nature of allosteric transitions: a plausible model. J Mol Biol. 1965; 12(1):88-118.